HHS Public Access

Author manuscript

Magn Reson Med. Author manuscript; available in PMC 2022 September 01.

Published in final edited form as:

Magn Reson Med. 2021 September ; 86(3): 1494–1504. doi:10.1002/mrm.28796.

Cardiac T_2* Measurement of Hyperpolarized ^{13}C Metabolites using Metabolite-Selective Multi-Echo Spiral Imaging

Junjie Ma[1], **Jun Chen**[1], **Galen D. Reed**[2], **Edward P. Hackett**[1], **Crystal E. Harrison**[1], **James Ratnakar**[1], **Rolf F. Schulte**[3], **Vlad G. Zaha**[1,4], **Craig R. Malloy**[1,4,5], **Jae Mo Park**[1,5,6]

[1]Advanced Imaging Research Center, The University of Texas Southwestern Medical Center, Dallas TX USA 75390

[2]GE Healthcare, Dallas, TX USA 75390

[3]GE Healthcare, Munich, Germany

[4]Internal Medicine, The University of Texas Southwestern Medical Center, Dallas TX USA 75390

[5]Radiology, The University of Texas Southwestern Medical Center, Dallas TX USA 75390

[6]Electrical and Computer Engineering, The University of Texas at Dallas, Richardson TX USA 75080

Abstract

Purpose: Noninvasive imaging with hyperpolarized pyruvate can capture *in vivo* cardiac metabolism. For proper quantification of the metabolites and optimization of imaging parameters, understanding MR characteristics such as T_2*s of the hyperpolarized signals is critical. This study is to measure *in vivo* cardiac T_2*s of hyperpolarized [1-^{13}C]pyruvate and the products in rodents and humans.

Methods: A dynamic ^{13}C multi-echo spiral imaging sequence that acquires [^{13}C]bicarbonate, [1-^{13}C]lactate, and [1-^{13}C]pyruvate images in an interleaved manner was implemented for a clinical 3T system. T_2* of each metabolite was calculated from the multi-echo images by fitting the signal decay of each region of interest mono-exponentially. The performance of measuring T_2* using the sequence was validated using a ^{13}C phantom, then with rodents following a bolus injection of hyperpolarized [1-^{13}C]pyruvate. In humans, T_2* of each metabolite was calculated for left ventricle (LV), right ventricle (RV) and myocardium.

Results: Cardiac T_2*s of hyperpolarized [1-^{13}C]pyruvate, [1-^{13}C]lactate and [^{13}C]bicarbonate in rodents were measured as 24.9 ± 5.0, 16.4 ± 4.7, and 16.9 ± 3.4 ms, respectively. In humans, T_2* of [1-^{13}C]pyruvate was 108.7 ± 22.6 ms in LV and 129.4 ± 8.9 ms in RV. T_2* of [1-^{13}C]lactate was 40.9 ± 8.3, 44.2 ± 5.5, and 43.7 ± 9.0 ms in LV, RV and myocardium, respectively. T_2* of [^{13}C]bicarbonate in myocardium was 64.4 ± 2.5 ms. The measurements were reproducible and consistent over time after the pyruvate injection.

Correspondence to: Jae Mo Park, Ph.D., The University of Texas Southwestern Medical Center, 5323 Harry Hines Blvd. Dallas TX 75019, jaemo.park@utsouthwestern.edu, +1-214-645-7206.

Conclusions: The proposed metabolite-selective multi-echo spiral imaging sequence reliably measures *in vivo* cardiac T_2*s of hyperpolarized [1-^{13}C]pyruvate and products.

Keywords

T_2*; multi-echo imaging; dynamic nuclear polarization; hyperpolarized pyruvate; heart

Introduction

MRI or MRS with hyperpolarized (HP) [1-^{13}C]pyruvate can assess metabolic state of the heart. In particular, detection of HP [^{13}C]bicarbonate is a direct measure of pyruvate dehydrogenase (PDH) activity and thus an important indicator of cardiac metabolism and function. For instance, myocardial [^{13}C]bicarbonate production is sensitive to several pathophysiological states, including myocardial infarction,[1] diabetic cardiomyopathy,[2] and heart failure.[3,4] Consequently, cardiac imaging with HP [1-^{13}C]pyruvate is being translated to humans.[5–7] Nonetheless, quantitative analysis of HP signals in the heart need to be established.

Cardiac imaging of HP signals is particularly challenging due to the cardiac motion and the rapid circulation of blood through the heart as well as the dynamic and transient nature of HP signals. To achieve rapid k-space sampling within a specific cardiac phase (e.g., end diastole), gradient recalled-echo (GRE)-based imaging sequences with spectral-spatial (spsp) radiofrequency (RF) pulses that excite one metabolite at a time are commonly used rather than spectroscopic imaging methods. Both spiral[5,8] or echo-planar imaging (EPI)[9,10] readouts were proposed for cardiac imaging previously.

However, cardiac HP acquisition schemes are still considered suboptimal,[11] and the HP ^{13}C images are sensitive to acquisition parameters such as echo times, B_0 field inhomogeneity[12,13] and blood flow.[14] For proper assessment of HP metabolites, *in vivo* MR characteristics such as the T_2*s of the HP ^{13}C-metabolites need to be understood. Moreover, since T_2*s play critical roles in determining acquisition parameters, the knowledge of the T_2* of HP [1-^{13}C]pyruvate and its products can be used in designing the k-space sampling trajectories for optimal signal-to-noise ratio (SNR) and spatial resolution. Previous studies estimated T_2*s of *in vivo* HP metabolites from the spectral linewidths using MR spectroscopy.[13] However, this approach measures aggregated T_2* information without assessing spatial and compartmental heterogeneity. A spectroscopic imaging approach, such as chemical shift imaging (CSI) or echo-planar spectroscopic imaging (EPSI), can be used to obtain spatial T_2* information of metabolites of interest by mapping the spectral linewidths,[15] but is not adequate for HP ^{13}C cardiac imaging due to the transient characteristics of HP signals and the relatively long acquisition time.

In this study, we propose a dynamic metabolite-selective multi-echo spiral imaging (MESI) ^{13}C sequence for imaging cardiac T_2*s of HP [1-^{13}C]pyruvate and the products *in vivo*. The feasibility and robustness of the method were validated using a ^{13}C phantom and tested with rodents *in vivo*. The sequence was further applied to healthy volunteers, and T_2* relaxation times of HP pyruvate, lactate, and bicarbonate were measured in left ventricle (LV), right ventricle (RV) and myocardium (Myo).

Methods

MR Scanner and RF coils

All the MR studies were performed using a clinical 3T wide-bore (diameter ⊘ = 70 cm) MRI scanner (750w Discovery, GE Healthcare, Waukesha, WI, USA). A $^{1}H/^{13}C$ dual-tuned quadrature transmit/receive birdcage RF coil (inner diameter $⊘_{inner}$ = 60 mm, GE Healthcare) was used for phantom and rat studies. For human studies, a two-loop ^{13}C transmit-receive Helmholtz coil was used (⊘ = 20 cm; PulseTeq Limited, Chobham, Surrey, UK). One loop was positioned over the anterior chest and the other was placed below the scapula of the human subject.

Hyperpolarization

A SPINlab™ system (GE Healthcare) that operates at ~0.8 K in a 5T magnet was used for the dynamic nuclear polarization (DNP) of [1-^{13}C]pyruvate. For animal studies, a 35-μL sample of 14-M [1-^{13}C]pyruvic acid mixed with OX063 trityl (15 mM) was prepared in a research fluid path for each dissolution. After 3 – 4 hrs of polarization, the sample was dissolved with hot solvent (16 mL saline with 0.1-g/L Na_2EDTA) then mixed with pH-neutralization media (750 μL with 0.72-M NaOH). The final HP solution (~6.5 mL) that contained ~70-mM of HP [1-^{13}C]pyruvate was injected through the tail vein up to 4.0 mL (0.875 mmol/kg body weight) with an injection rate of 0.25 mL/s.

For human studies, [1-^{13}C]pyruvic acid (Sigma Aldrich, St. Louis, MO), produced in accordance with Good Manufacturing Practice (GMP) regulations, was prepared in clinical fluid paths as described previously (0.40 mL/kg body weight of 250-mM HP [1-^{13}C]pyruvate solution).[16] HP [1-^{13}C]pyruvate was dissolved after 3 – 4 hrs of polarization. Pyruvate concentration, pH, temperature, volume and radical concentration of the HP solution was examined by a dedicated quality control (QC) device (GE Healthcare). Immediately after passing the QC, sterility of the sample was confirmed prior to injection as previously described.[17] The HP solution was transported to the magnet and administered intravenously to subjects (injection rate = 5 mL/s), followed by a 25-mL saline flush.

RF Pulse Design and Metabolite-Interleaved Multi-Echo Spiral Imaging Sequence

A spsp RF pulse was designed to have a full width at half maximum (FWHM) of 134.4 Hz using the Spectral-Spatial RF Pulse Design Package[18] to selectively excite HP [^{13}C]bicarbonate, [1-^{13}C]lactate, or [1-^{13}C]pyruvate, depending on the acquisition frequency, Fig. 2. Unlike other spsp RF pulses used in previous HP ^{13}C cardiac studies,[5,8,9] this RF pulse was specifically designed and tested for the wide-bore system (GE 750w), which has limited gradient performance (maximum gradient [G_{max}] = 33 mT/m, maximum slew rate [$Slew_{max}$] = 120 T/m/s), and operates with minimum gradient requirements (G_{max} < 25 mT/m and $Slew_{max}$ < 100 T/m/s). The spsp excitation profiles, simulated using MATLAB (MathWorks, Natick, MA, USA) and tested in the scanner, are shown in Fig. 2(B). The simulated transverse signal in log scale at the center of the image slice (horizontal dotted white line) showed 90° excitation in the passband and less than 1% excitation in the stopband. Metabolite-selective MESI scheme was implemented to sequentially acquire

metabolite maps using the spsp RF pulse in an interleaved manner by shifting the transmit and receive frequencies.

Phantom Validation

The sequence was tested with a gadolinium-doped (1-mM) spherical [^{13}C]bicarbonate phantom (1.0 M, ∅ = 3 cm). ^{1}H MRI was acquired with two-dimensional (2D) T_1-weighted fast spin echo (FSE) sequence (repetition time [TR] = 700 ms, echo time [TE] = 12 ms, flip angle [FA] = 90°, field of view [FOV] = 60 mm × 60 mm, slice thickness [ST] = 4 mm, spatial resolution = 0.23 mm × 0.23 mm). For ^{13}C MRI, five-echo images of each metabolite were acquired following the spsp RF excitation with two-shot spiral readouts (FOV = 60 mm × 60 mm, spatial resolution = 3 mm × 3 mm, FA = 90°, ST = 25 mm, TR = 3 s, TE of 1st echo = 18.01 ms, ΔTE = 11.62 ms, readout length = 58.10 ms/arm, receiver spectral bandwidth = 85.06 Hz, #averages = 128). The decay of mean ^{13}C signal within the phantom was fitted to a mono-exponential function to measure the T_2* of [^{13}C]bicarbonate. From the same phantom, ^{13}C spectrum was acquired using a pulse-and-acquire sequence (FA = 90°, ST = 25 mm, TR = 3 s, receive spectral bandwidth = 2000 Hz, total #spectral points = 2048, #averages = 128). The T_2* from the MESI was compared to the linewidth from the spectroscopic data. In the frequency domain, the ideal MRS signal can be described by the Lorentzian line shape,[15] which is in the form as below in magnitude:

$$S(f) = \frac{H}{\sqrt{W^2 + (F_0 - f)^2}} \quad \#(1)$$

where H is the maximum of the signal in magnitude, F_0 is the center frequency, and W is the signal's FWHM ($W = \frac{1}{\pi T_2^*}$). T_2* of the phantom was calculated by fitting the spectrum to Equation (1).

T_2* Measurement of Rat Heart

Cardiac T_2*s of HP ^{13}C-metabolites were measured from healthy male Wistar rats (n = 3, body weight = 556.7 ± 64.7 g). First, 2D axial T_2-weighted FSE ^{1}H images were acquired for anatomical reference (TR = 5000 ms, TE = 63 ms, FA = 160°, FOV = 80 mm × 80 mm, ST = 2 mm, spatial resolution = 0.63 mm × 0.63 mm). Each rat was imaged twice using the ^{13}C MESI sequence (single shot, FOV = 80 mm × 80 mm, spatial resolution = 8 mm × 8 mm, ST = 25 mm, TR = 213 ms, #echo = 10, TE of 1st echo = 15.19 ms, ΔTE = 5.98 ms, readout length = 59.76 ms/arm, receive spectral bandwidth = 167.34 Hz, FA = 90° for bicarbonate, 90° for lactate, and 5° for pyruvate, #timepoint = 16) with two consecutive injections of HP [1-^{13}C]pyruvate solution. Images of [^{13}C]bicarbonate, [1-^{13}C]lactate, and [1-^{13}C]pyruvate were acquired from an axial plane containing the heart after a 15-s delay from the start of each injection. The minimum time interval between the injections was 20 min. The acquisition scheme is summarized in Fig. 1. Note that the ECG gating was used only for humans. All procedures were approved by the local Institutional Animal Care and Use Committee.

Cardiac T_2* Measurement of Healthy Human Subjects

Three healthy subjects were recruited for the study (2 female, 1 male, age = 38 – 48 years, Table 1). After positioning the subject in the magnet, horizontal long-axis (HLA), vertical long-axis (VLA) and short-axis (SA) images were acquired using a ^{1}H balanced steady-state free precession (bSSFP) sequence, which was triggered to mid-diastole during expiration breath-hold. B_0 inhomogeneity was inspected in a mid LV SA plane using a ^{1}H GRE (FOV = 400 mm × 400 mm, spatial resolution = 6.25 mm × 6.25 mm, 2 echoes with ΔTE = 3.30 ms, TE of 1st echo = 2.80 ms) with breath-hold (no cardiac triggering). The SA plane and the shim currents were retained for ^{13}C imaging. The HP ^{13}C images were acquired with ECG gating. The scanning sequence began after a 25-s delay from the start of pyruvate injection using an automated breath-hold voice instruction given immediately before the scan. Subjects were instructed to hold their breath in expiration for ~20 s, followed by a shallow breathing to minimize the respiratory motion. The center frequency was set to the *in vivo* HP [^{13}C]bicarbonate resonance, which was predetermined by the *in vivo* HP [1-^{13}C]lactate frequency, and the center frequency of water protons was used to calculate the frequency of [1-^{13}C]lactate with an empirically-derived scaling factor of 0.2514949. The multi-echo images of [^{13}C]bicarbonate, [1-^{13}C]lactate and [1-^{13}C]pyruvate were acquired in an interleaved manner every 2 R-R intervals (single shot, FOV = 400 mm × 400 mm, spatial resolution = 16 mm × 16 mm, ST = 30 mm, #echo = 6, TE of 1st echo = 16.99 ms, ΔTE = 9.59 ms, readout length = 57.53 ms/arm, receive spectral bandwidth = 104.4 Hz, FA = 60° for bicarbonate, 60° for lactate, and 20° for pyruvate, #timepoint = 16). The imaging protocol was approved by the local Institutional Review Board (IRB#: STU-2018–0227).

Data Reconstruction and Statistical Analysis

All the acquired HP ^{13}C data were reconstructed and analyzed using MATLAB. Images from different echoes were reconstructed by inverse Fourier transform after gridding to Cartesian coordinates, apodization with a Gaussian function, sample density compensation, and a four-fold zero-filling in k-space. To combine the multi-echo data, images from all echoes were added with equal weights.

Off-resonance correction for the HP ^{13}C images was conducted with a frequency-segmented method as described in.[19] The data was demodulated over a range of off-resonance frequencies from −50 Hz to 50 Hz in 5 Hz step. From each of the resultant images, pixels whose field map values most closely match the reconstruction frequency were selected to form the final image. The ^{13}C field map was estimated from the ^{1}H field map, which firstly passed a median filter (3 × 3) to eliminate noise spikes and was then resampled to the resolution of ^{13}C image and scaled by the ratio of $\frac{\gamma_{^{13}C}}{\gamma_{^{1}H}}$.

For the animal data, regions of interest (ROIs) that contain hyperintense ^{13}C signals were drawn in the ^{13}C images, and the mean ^{13}C signal within each ROI was fitted to an exponential decaying function along the echo times to calculate the T_2*s of HP [^{13}C]bicarbonate, [1-^{13}C]lactate and [1-^{13}C]pyruvate. Paired Student's t-test ($\alpha = 0.05$, two-tailed) was performed between the consecutively measured T_2*s of HP metabolites to verify

the reproducibility of the proposed method. Dynamic change of the T_2* measurements along the timepoints was evaluated by the coefficient of variation (CV).

For the human ^{13}C data, LV, RV, and Myo were manually segmented based on the ^{1}H SA MRI, as shown in Fig. 7(A). The spatially averaged ^{13}C signals over the compartments at each echo were used to calculate the compartmentalized T_2*s in the heart. To ensure the accuracy of T_2* measurement, signals from the first m echoes (m = 3 or 4, depending on the SNR) were used for linear regression with the premise that coefficients of determination (r^2) for the linear regressions of first m and $m+1$ echoes are both larger than 0.95.

To evaluate the improvement of SNR with the sequence, peak SNRs from the first-echo and echo-combined HP ^{13}C images were calculated by:

$$SNR_{peak} = \frac{s_{max} - mean(n)}{std(n)} \quad \#(2)$$

where s_{max} is the maximum signal of the image and n is the background noise. For human images, SNR maps were also reported for both first-echo and echo-combined images.

Results

^{1}H MRI and ^{13}C images of the [^{13}C]bicarbonate phantom are shown in Fig. 3(A). The T_2* calculated from the multi-echo images was 54.5 ms (r^2 = 0.99), Fig. 3(B). T_2* of the phantom was estimated as 54.0 ms using the Lorentzian fitting (red dotted line) of the acquired spectrum (blue solid line) in magnitude as in Fig. 3(C).

Time-resolved (15 – 40 s from the start of injection) cardiac ^{13}C images of HP [1-^{13}C]pyruvate, [1-^{13}C]lactate and [^{13}C]bicarbonate from a representative rat are shown in Fig. 4. The echo-combined ^{13}C images are overlaid on top of the corresponding ^{1}H image (Fig. 4(A)). ^{1}H Δf_0 map of the imaging slice is shown in Fig. 4(B). Strong pyruvate and lactate signals were detected from the LV, and a large bicarbonate signal was observed in the left anterior Myo, as previously reported.[9,10] The cardiac T_2* of HP [1-^{13}C]pyruvate was measured as 24.9 ± 5.0 ms. T_2*s of [1-^{13}C]lactate and [^{13}C]bicarbonate were 16.4 ± 4.7 and 16.9 ± 3.4 ms, respectively.

Individual echo images could be also resolved at each timepoint. The first six echo images at the second timepoint (20 s post-injection), for instance, are shown in Fig. 5(A) from the representative rat. Changes of spatially-averaged ^{13}C signals along the echo time are displayed in Fig. 5(B) for selected ROIs (solid black squares in Fig. 5(A)). For [1-^{13}C]pyruvate and [1-^{13}C]lactate, the mean ^{13}C signals in the first four echoes were used for linear regression. For HP [^{13}C]bicarbonate, the first three echoes were used due to the limited SNR in the images with longer echoes. The T_2*s of [1-^{13}C]pyruvate, [1-^{13}C]lactate and [^{13}C]bicarbonate were 27.3 ms (r^2 = 0.99), 9.5 ms (r^2 = 0.99) and 13.9 ms (r^2 = 0.99), respectively, at 20 s post-injection (Fig. 5B) from the representative rat.

T_2*s were consistent over time (CV < 0.23). From the representative rat, the time-averaged T_2*s of [1-^{13}C]pyruvate, [1-^{13}C]lactate, and [^{13}C]bicarbonate were measured as 25.0 ± 3.5,

12.9 ± 2.2, and 14.8 ± 1.1 ms, respectively, as shown in Fig. 5(C). No significant difference was found from the two consecutive measurements of time-averaged T_2*s, as summarized in Fig. 6.

For HP ^{13}C cardiac imaging of healthy subjects, pyruvate and lactate signals were primarily detected in LV and RV while bicarbonate was preserved in Myo, which is consistent with a previous report.[5] T_2* of HP [1-^{13}C]pyruvate was 108.7 ± 22.6 ms in LV and 129.4 ± 8.9 ms in RV. T_2* of [1-^{13}C]pyruvate in Myo was not calculated due to the low SNR. [1-^{13}C]Lactate T_2* was measured as 40.9 ± 8.3 ms in LV, 44.2 ± 5.5 ms in RV, and 43.7 ± 9.0 ms in Myo. T_2* of [^{13}C]bicarbonate was reliable only in Myo and measured as 64.4 ± 2.5 ms, which is within the range of previous measurement from human heart (T_2* = 58 ± 20 ms) using the spectral linewidth of HP [^{13}C]bicarbonate.[13] Time-averaged T_2*s from individual subjects are summarized in Table 1. Fig. 7 shows HP ^{13}C metabolite maps from a representative subject (subject 1). As shown in Fig. 7(C), HP [1-^{13}C]pyruvate, [1-^{13}C]lactate, and [^{13}C]bicarbonate images were acquired at multiple timepoints, and multi-echo images at each timepoint were examined for T_2* estimation (Fig. 8). From the subject, T_2*s of [1-^{13}C]pyruvate and [1-^{13}C]lactate were 85.7 ms (r^2 = 0.99) and 56.6 ms (r^2 = 0.98), respectively, in LV at 25 s post-injection. In RV, the T_2*s of [1-^{13}C]pyruvate and [1-^{13}C]lactate were 164.2 ms (r^2 = 0.98) and 42.9 ms (r^2 = 0.99), respectively. T_2*s of [1-^{13}C]lactate and [^{13}C]bicarbonate in Myo was 49.2 ms (r^2 = 0.95) and 63.6 ms(r^2 = 0.97), respectively. T_2*s were consistent over the timepoints for all the HP metabolites (CV < 0.21), as shown in Fig. 8(C). The QC measured that the pyruvate concentration in the final solution was 248.3 ± 11.2 mM with 0.4 ± 0.3 μM residual radical. The liquid-state polarization level was measured as 33.5% ± 9.6%. The dissolution to injection time was 64.7 ± 3.8 s.

Although T_2*-weighted, multi-echo images of HP metabolite maps can be combined to improve the SNR, the improvements varied for different metabolites depending on the T_2*s and the initial SNRs of the first-echo images. In animals, the peak SNRs of the echo-combined ^{13}C images increased by 44 ± 22 %, 29 ± 23 %, and 28 ± 22 % compared to those of the first-echo images for [^{13}C]bicarbonate, [1-^{13}C]lactate and [1-^{13}C]pyruvate, respectively. In humans, the peak SNRs increased by 135 ± 22 % for [^{13}C]bicarbonate, 42 ± 18 % for [1-^{13}C]lactate, and 105 ± 33 % for [1-^{13}C]pyruvate. The echo-combined SNR improvements are summarized in Supporting Information Fig. S1.

Discussion

In this study, we implemented ECG-gated metabolite-selective ^{13}C MESI sequence for cardiac T_2* mapping of HP metabolites. The feasibility and the reproducibility of T_2* measurement using the proposed method was validated in a phantom and animals. In humans, T_2*s of HP ^{13}C-metabolites could be spatially resolved for LV, RV and Myo despite the limited spatial resolution due to the short echo-spacing and the compromised gradient performance of the wide-bore system.

Contributing Factors to T_2*s of HP ^{13}C Metabolites

The T_2* values were reported in the heart for three HP metabolites: [1-^{13}C]pyruvate, [1-^{13}C]lactate and [^{13}C]bicarbonate. The distinct T_2* values could originate from several contributing factors such as off-resonance, blood flow, and T_2, in addition to acquisition parameters. The off-resonance could be from the spatial inhomogeneity of B_0 or inaccurate assignment of acquisition frequencies for each metabolite. Comparing the T_2*s measured from rat and human hearts, the longer T_2*s of HP metabolites in human heart may arise from the more homogeneous B_0 field (e.g., better shimming) due to the slower heart rate and the presence of ECG gating. (R2.9) Likewise, the inter-subject variance of B_0 inhomogeneities may explain the relatively wide distribution of T_2*s in rats, as shown in Fig. 6. Pyruvate had significantly longer T_2*s than lactate ($p < 0.0001$) and bicarbonate ($p < 0.001$); this is likely due to the T_2 difference between HP metabolites. Indeed, a previous rat study reported longer T_2 for [1-^{13}C]pyruvate compared to [1-^{13}C]lactate in the liver.[20] Moreover, it was noted that T_2*s of HP [1-^{13}C]pyruvate and [1-^{13}C]lactate were longer in RV compared to those in LV (Table 1). The difference could be related to the higher filling velocity in LV than RV.[21] Flow-induced signal decay is strong in LV, resulting in shorter T_2*s for HP [1-^{13}C]pyruvate and [1-^{13}C]lactate in LV than RV. On the contrary, the relatively long T_2* of HP [^{13}C]bicarbonate in Myo is likely due to the absence of the blood flow effect.

Improved Assessment of Cardiac HP Signals

For most HP studies, utility of measured HP T_2*s lies primarily in accurate quantification of HP signals. In particular, understanding T_2* effect is crucial for appropriate assessment of HP data acquired by GRE-based pulse sequences and the design of the readout trajectories. Previous efforts to compensate the T_2* effect in HP ^{13}C images have been focused on the off-resonance effect. Reed, *et al.* demonstrated improved B_0 shimming to mitigate the non-uniform circumferential HP [^{13}C]bicarbonate signal from the Myo.[13] Traechtler, *et al.* proposed a model-based reconstruction to correct the B_0-induced phase offsets in HP ^{13}C multi-echo acquisition.[12] Considering the other contributing factors besides off-resonance effect, direct measurements of *in vivo* T_2* would further benefit the cardiac HP ^{13}C studies.

Potential Improvements and Applications

In this study, in-plane spatial resolution of *in vivo* HP studies was compromised due to SNR available and the echo time needed for accurate T_2* measurement. The partial volume effect may cause mismatch between the segmentation from ^{1}H MRI and actual ^{13}C signal distribution, leading to inaccurate measurement of T_2*. The low in-plane resolution could also result in sub-optimal T_2* maps. Therefore, in this study, we took the spatially averaged signal for T_2* fitting instead of the voxel-by-voxel analysis to insure the accurate measurement of T_2*. For future work, multi-shot spiral readout can be considered with carefully designed excitation angle strategy.[22] Alternatively, acceleration techniques such as parallel imaging[23] and compressed sensing[24] can also be integrated into the MESI sequence for improving spatial resolution.

In the rat studies, cardiac gating was not available for HP imaging, resulting in motion artifacts in the ^{13}C images. By carefully choosing ROIs for the mean signal quantification,

we were able to mitigate the impact from the artifact, while it would be beneficial to include cardiac gating or respiratory control for animal study in the future.

Several aspects of T_2*s in HP metabolites need further investigation. For instance, flow contribution to the T_2* can be clarified by utilizing flow-sensitive gradients.[25] Moreover, it should be noted that the T_2*s depend on acquisition parameters such as the size[26,27] and the shape[27] of the voxel, the slice thickness,[28] eddy currents.[29]

As HP pyruvate is utilized to study metabolism in various *in vivo* applications,[30–32] T_2*s of HP ^{13}C metabolites in other organs and tissue types will be beneficial for establishing optimized k-space sampling patterns. In particular, large variation of magnetic susceptibility is expected in pathological states such as glioblastoma[33] due to blood depositions and calcifications, leading to potential underestimation of HP signals.

In vivo T_2 is another under-explored feature of HP molecules.[20,34,35] Yen, *et al.* reported nearly 1-second-long T_2s of HP signals with potentially unique metabolic contrast in rat hepatocellular carcinoma.[20] Joe, *et al.* estimated *in vivo* T_2s of HP ^{13}C-metabolites by combining the ^{1}H B_0 map and ^{13}C T_2* maps.[35] Due to the complex T_2* relaxation mechanism of HP ^{13}C-metabolites, T_2 calculation using ^{1}H B_0 map will need further verification.

Conclusions

In conclusion, we proposed a ^{13}C multi-echo spiral imaging sequence to measure *in vivo* cardiac T_2*s of HP [1-^{13}C]pyruvate and its products. A phantom test and *in vivo* animal studies validated the method is robust and reproducible. Cardiac T_2*s of HP [1-^{13}C]pyruvate, [1-^{13}C]lactate and [^{13}C]bicarbonate at 8 mm × 8 mm spatial resolution in rodents were measured as 24.9 ± 5.0, 16.4 ± 4.7, and 16.9 ± 3.4 ms, respectively. T_2*s of the HP ^{13}C-metabolites at 16 mm × 16 mm spatial resolution in human heart are observed as 108.7 ± 22.6 ms (LV) and 129.4 ± 8.9 ms (RV) for [1-^{13}C]pyruvate, 40.9 ± 8.3 ms (LV), 44.2 ± 5.5 ms (RV) and 43.7 ± 9.0 ms (Myo) for [1-^{13}C]lactate, and 64.4 ± 2.5 ms (Myo) for [^{13}C]bicarbonate.

Supplementary Material

Refer to Web version on PubMed Central for supplementary material.

Acknowledgements

Personnel Support:

We appreciate the clinical research team and the supporting staffs of the Advanced Imaging Research Center at UT Southwestern for imaging the volunteers - Jeff Liticker, PharmD, Ronald G. Hall, PharmD, Jaffar Raza, PharmD, Jeannie Baxter, RN, Kelley Derner, RN, Salvador Pena, Corey Mozingo, Maida Tai, and Richard Martin.

Funding:

National Institutes of Health of the United States (P41 EB015908, S10 RR029119, S10 OD018468, R01 NS107409); The Welch Foundation (I-2009-20190330); UT Dallas Collaborative Biomedical Research Award (UTD 1907789); The Cancer Prevention and Research Institute of Texas (RP180404). The Texas Institute for Brain Injury and Repair.

References

1. Golman K, Petersson JS, Magnusson P, et al. Cardiac metabolism measured noninvasively by hyperpolarized ^{13}C MRI. Magn Reson Med. 2008;59:1005–1013. [PubMed: 18429038]
2. Le Page LM, Rider OJ, Lewis AJ, et al. Increasing pyruvate dehydrogenase flux as a treatment for diabetic cardiomyopathy: a combined ^{13}C hyperpolarized magnetic resonance and echocardiography study. Diabetes. 2015;64:2735–2743. [PubMed: 25795215]
3. Agger P, Hyldebrandt JA, Hansen ESS, et al. Magnetic resonance hyperpolarization imaging detects early myocardial dysfunction in a porcine model of right ventricular heart failure. Eur Heart J Cardiovasc Imaging. 2020;21:93–101. [PubMed: 31329841]
4. Schroeder MA, Lau AZ, Chen AP, et al. Hyperpolarized ^{13}C magnetic resonance reveals early- and late-onset changes to in vivo pyruvate metabolism in the failing heart. Eur J Heart Fail. 2013;15:130–140. [PubMed: 23258802]
5. Cunningham CH, Lau JYC, Chen AP, et al. Hyperpolarized ^{13}C metabolic MRI of the human heart: initial experience. Circ Res. 2016;119:1177–1182. [PubMed: 27635086]
6. Rider OJ, Apps A, Miller JJJJ, et al. Noninvasive in vivo assessment of cardiac metabolism in the healthy and diabetic human heart using hyperpolarized ^{13}C MRI. Circ Res. 2020;126:725–736. [PubMed: 32078413]
7. Park JM, Reed GD, Liticker J, et al. Effect of doxorubicin on myocardial bicarbonate production from pyruvate dehydrogenase in women with breast cancer. Circ Res. 2020;127:1568–1570. [PubMed: 33054563]
8. Lau AZ, Chen AP, Ghugre NR, et al. Rapid multislice imaging of hyperpolarized ^{13}C pyruvate and bicarbonate in the heart. Magn Reson Med. 2010;64:1323–1331. [PubMed: 20574989]
9. Miller JJ, Lau AZ, Teh I, et al. Robust and high resolution hyperpolarized metabolic imaging of the rat heart at 7 T with 3D spectral-spatial EPI. Magn Reson Med. 2016;75:1515–1524. [PubMed: 25991606]
10. Wespi P, Steinhauser J, Kwiatkowski G, Kozerke S. High-resolution hyperpolarized metabolic imaging of the rat heart using k-t PCA and k-t SPARSE. NMR Biomed. 2018;31:e3876.
11. Malloy CR, Sherry AD. Biochemical specificity in human cardiac imaging by ^{13}C magnetic resonance imaging. Circ Res. 2016;119:1146–1148. [PubMed: 28051774]
12. Traechtler J, Vishnevskiy V, Fuetterer M, Dounas A, Kozerke S. Joint image and field map estimation for multi-echo hyperpolarized ^{13}C metabolic imaging. In Proceedings of the 2020 ISMRM & SMRT Virtual Conference & Exhibition. #3016.
13. Reed GD, Ma J, Park JM, et al. Characterization and compensation of f_0 inhomogeneity artifact in spiral hyperpolarized ^{13}C imaging of the human heart. Magn Reson Med. 2021;00:1–10.
14. Wespi P, Steinhauser J, Kwiatkowski G, Kozerke S. Overestimation of cardiac lactate production caused by liver metabolism of hyperpolarized [1-^{13}C]pyruvate. Magn Reson Med. 2018;80:1882–1890. [PubMed: 29607535]
15. Alger JR. Quantitative proton magnetic resonance spectroscopy and spectroscopic imaging of the brain: a didactic review. Top Magn Reson Imaging. 2010;21:115–128. [PubMed: 21613876]
16. Nelson SJ, Kurhanewicz J, Vigneron DB, et al. Metabolic imaging of patients with prostate cancer using hyperpolarized [1-^{13}C]pyruvate. Sci Transl Med. 2013;5:198ra108.
17. Park I, Larson PEZ, Gordon JW, et al. Development of methods and feasibility of using hyperpolarized carbon-13 imaging data for evaluating brain metabolism in patient studies. Magn Reson Med. 2018;80:864–873. [PubMed: 29322616]
18. Larson PEZ, Kerr AB, Chen AP, et al. Multiband excitation pulses for hyperpolarized ^{13}C dynamic chemical-shift imaging. J Magn Reson. 2008;194:121–127. [PubMed: 18619875]
19. Man LC, Pauly JM, Macovski A. Multifrequency interpolation for fast off-resonance correction. Magn Reson Med. 1997;37:785–792. [PubMed: 9126954]
20. Yen Y-F, Le Roux P, Mayer D, et al. T_2 relaxation times of ^{13}C metabolites in a rat hepatocellular carcinoma model measured in vivo using ^{13}C-MRS of hyperpolarized [1-^{13}C]pyruvate. NMR Biomed. 2010;23:414–423. [PubMed: 20175135]

21. Haddad F, Hunt SA, Rosenthal DN, Murphy DJ. Right ventricular function in cardiovascular disease, part I: anatomy, physiology, aging, and functional assessment of the right ventricle. Circulation. 2008;117:1436–1448. [PubMed: 18347220]
22. Walker CM, Fuentes D, Larson PEZ, Kundra V, Vigneron DB, Bankson JA. Effects of excitation angle strategy on quantitative analysis of hyperpolarized pyruvate. Magn Reson Med. 2019;81:3754–3762. [PubMed: 30793791]
23. Arunachalam A, Whitt D, Fish K, et al. Accelerated spectroscopic imaging of hyperpolarized C-13 pyruvate using SENSE parallel imaging. NMR Biomed. 2009;22:867–873. [PubMed: 19489035]
24. Geraghty BJ, Lau JYC, Chen AP, Cunningham CH. Accelerated 3D echo-planar imaging with compressed sensing for time-resolved hyperpolarized ^{13}C studies. Magn Reson Med. 2017;77:538–546. [PubMed: 26806525]
25. Gordon JW, Niles DJ, Adamson EB, Johnson KM, Fain SB. Application of flow sensitive gradients for improved measures of metabolism using hyperpolarized ^{13}c MRI. Magn Reson Med. 2016;75:1242–1248. [PubMed: 25951611]
26. Fernndez-Seara MA, Wehrli FW. Postprocessing technique to correct for background gradients in image-based R^*_2 measurements. Magn Reson Med. 2000;44:358–366. [PubMed: 10975885]
27. Yablonskiy DA, Haacke EM. Theory of NMR signal behavior in magnetically inhomogeneous tissues: the static dephasing regime. Magn Reson Med. 1994;32:749–763. [PubMed: 7869897]
28. Reeder SB, Faranesh AZ, Boxerman JL, McVeigh ER. In vivo measurement of T_2* and field inhomogeneity maps in the human heart at 1.5 T. Magn Reson Med. 1998;39:988–998. [PubMed: 9621923]
29. Josan S, Kaye E, Pauly JM, Daniel BL, Pauly KB. Improved half RF slice selectivity in the presence of eddy currents with out-of-slice saturation. Magn Reson Med. 2009;61:1090–1095. [PubMed: 19319972]
30. Grist JT, McLean MA, Riemer F, et al. Quantifying normal human brain metabolism using hyperpolarized [1-^{13}C]pyruvate and magnetic resonance imaging. Neuroimage. 2019;189:171–179. [PubMed: 30639333]
31. Gallagher FA, Woitek R, McLean MA, et al. Imaging breast cancer using hyperpolarized carbon-13 MRI. Proc Natl Acad Sci USA. 2020;117:2092–2098. [PubMed: 31964840]
32. Tang S, Bok R, Qin H, et al. A metabolite-specific 3D stack-of-spiral bSSFP sequence for improved lactate imaging in hyperpolarized [1-^{13}C]pyruvate studies on a 3 T clinical scanner. Magn Reson Med. 2020;84:1113–1125. [PubMed: 32086845]
33. Deistung A, Schweser F, Wiestler B, et al. Quantitative susceptibility mapping differentiates between blood depositions and calcifications in patients with glioblastoma. PLoS One. 2013;8:e57924. [PubMed: 23555565]
34. Milshteyn E, Reed GD, Gordon JW, et al. Simultaneous T_1 and T_2 mapping of hyperpolarized ^{13}C compounds using the bSSFP sequence. J Magn Reson. 2020;312:106691. [PubMed: 32058912]
35. Joe E, Lee H, Lee J, et al. An indirect method for in vivo T_2 mapping of [1-^{13}C]pyruvate using hyperpolarized ^{13}C CSI. NMR Biomed. 2017;30:e3690.

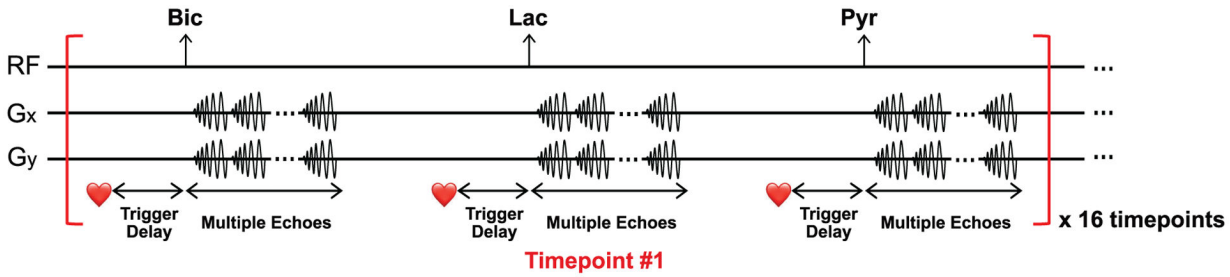

Figure 1. Metabolite-interleaved ^{13}C multi-echo spiral imaging sequence.

[^{13}C]Bicarbonate, [1-^{13}C]lactate and [1-^{13}C]pyruvate are sequentially excited using a spectral-spatial RF pulse and imaged with multiple single-shot spiral readouts.

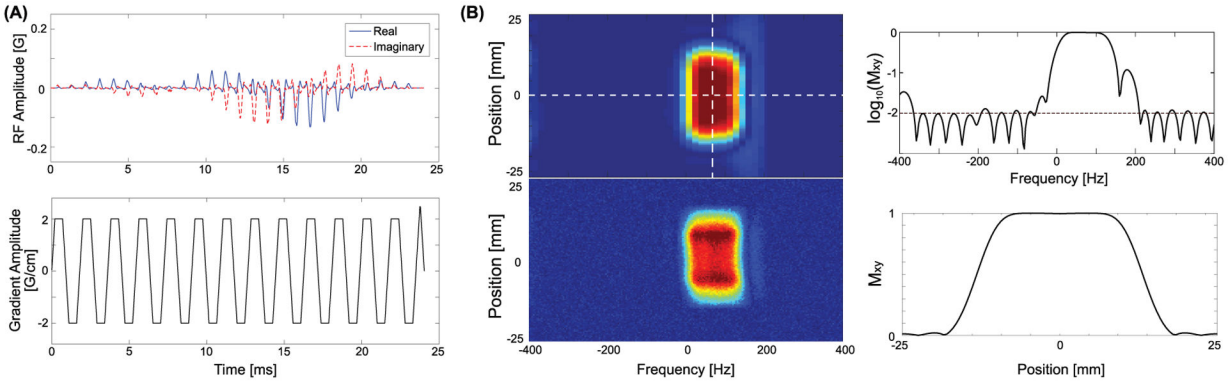

Figure 2. Spectral-spatial RF pulse and profiles.

(A) Spectral-spatial RF pulse and slice-selective gradient waveforms used for bicarbonate, lactate, and pyruvate excitation, and (B) the simulated (top left) and tested (bottom left) excitation profile. The simulated spectral profile at the center of the slice (horizontal dotted white line in the top left figure) in log scale is shown at the top right, and the simulated slice profile at the center of the passing band (vertical dotted white line in the top left figure) is shown at the bottom right.

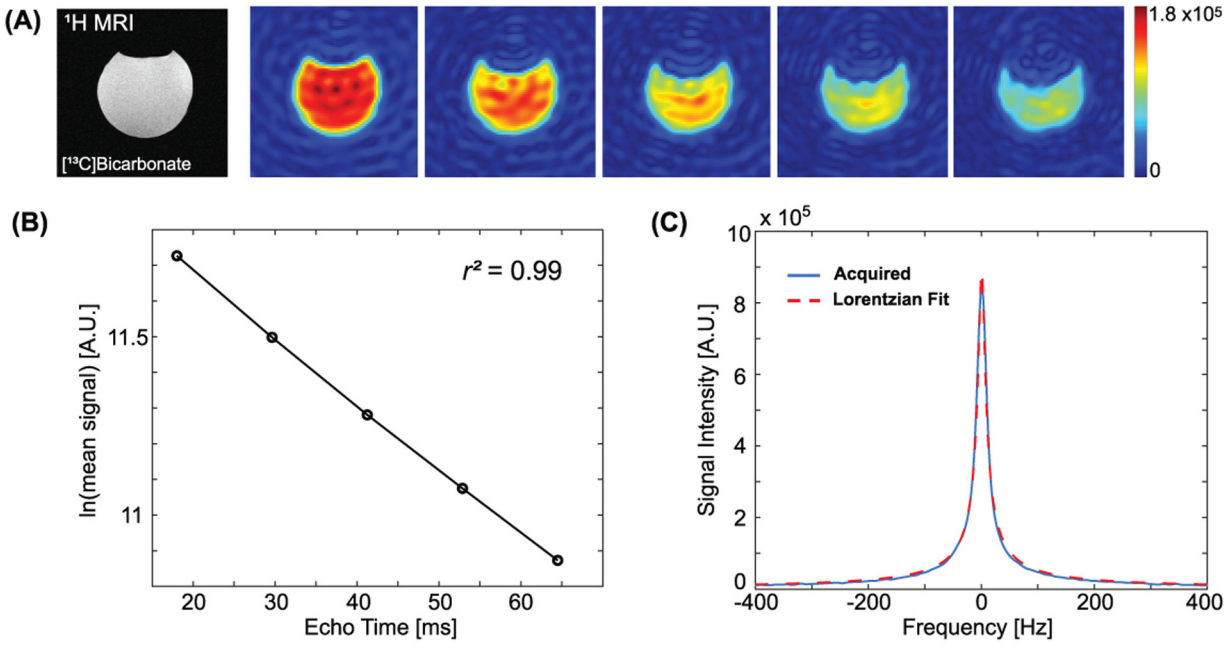

Figure 3. Phantom evaluation.

(A) Performance evaluation of the pulse sequence using a [^{13}C]bicarbonate phantom. The T_2* from the MESI sequence (B) was compared to that from the Lorentzian fit of ^{13}C spectrum (C).

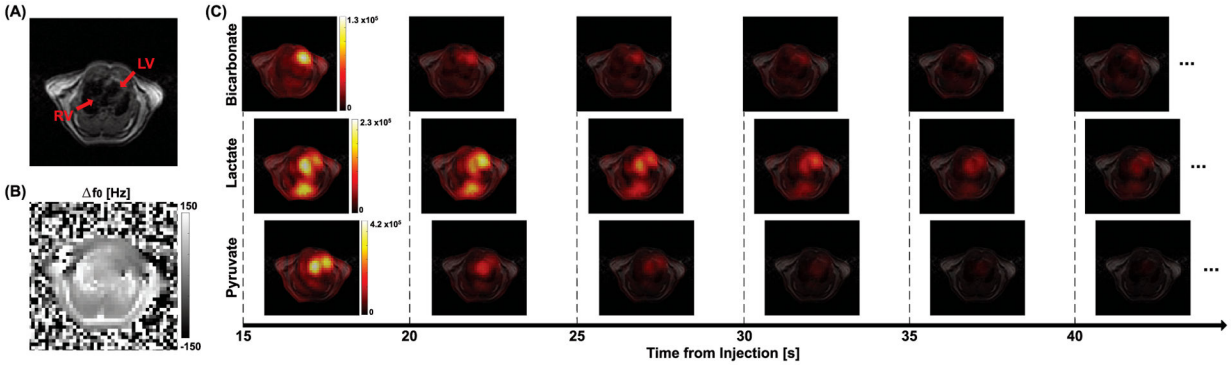

Figure 4. Hyperpolarized ^{13}C imaging from a representative rat.

An axial slice that includes the heart was prescribed for both ^{1}H and ^{13}C MRI. (A) T_2-weighted image and (B) Δf_0 map were acquired in ^{1}H. (C) Multi-echo images (10 echoes) of [1-^{13}C]pyruvate, [1-^{13}C]lactate and [^{13}C]bicarbonate were acquired every 5 s after an injection of HP [1-^{13}C]pyruvate, and combined at each timepoint.

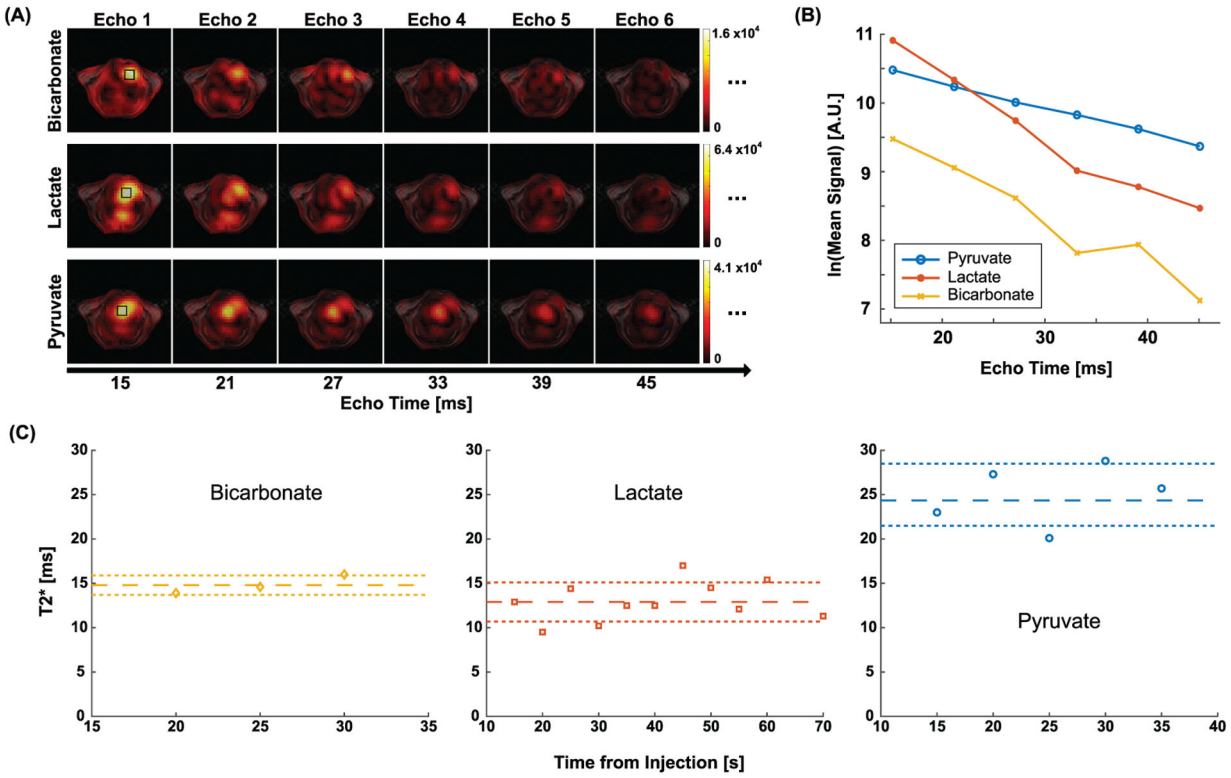

Figure 5. ***In vivo*** **cardiac T_2* measurement from the representative rat.**

(A) The first six echo images of [1-^{13}C]pyruvate, [1-^{13}C]lactate and [^{13}C]bicarbonate at 20 s. (B) Signal decay of HP ^{13}C metabolites in the ROI (black squares in (C)) along echo time. (C) T_2*s of HP signals at different timepoints. The reference lines denote mean ± standard deviation.

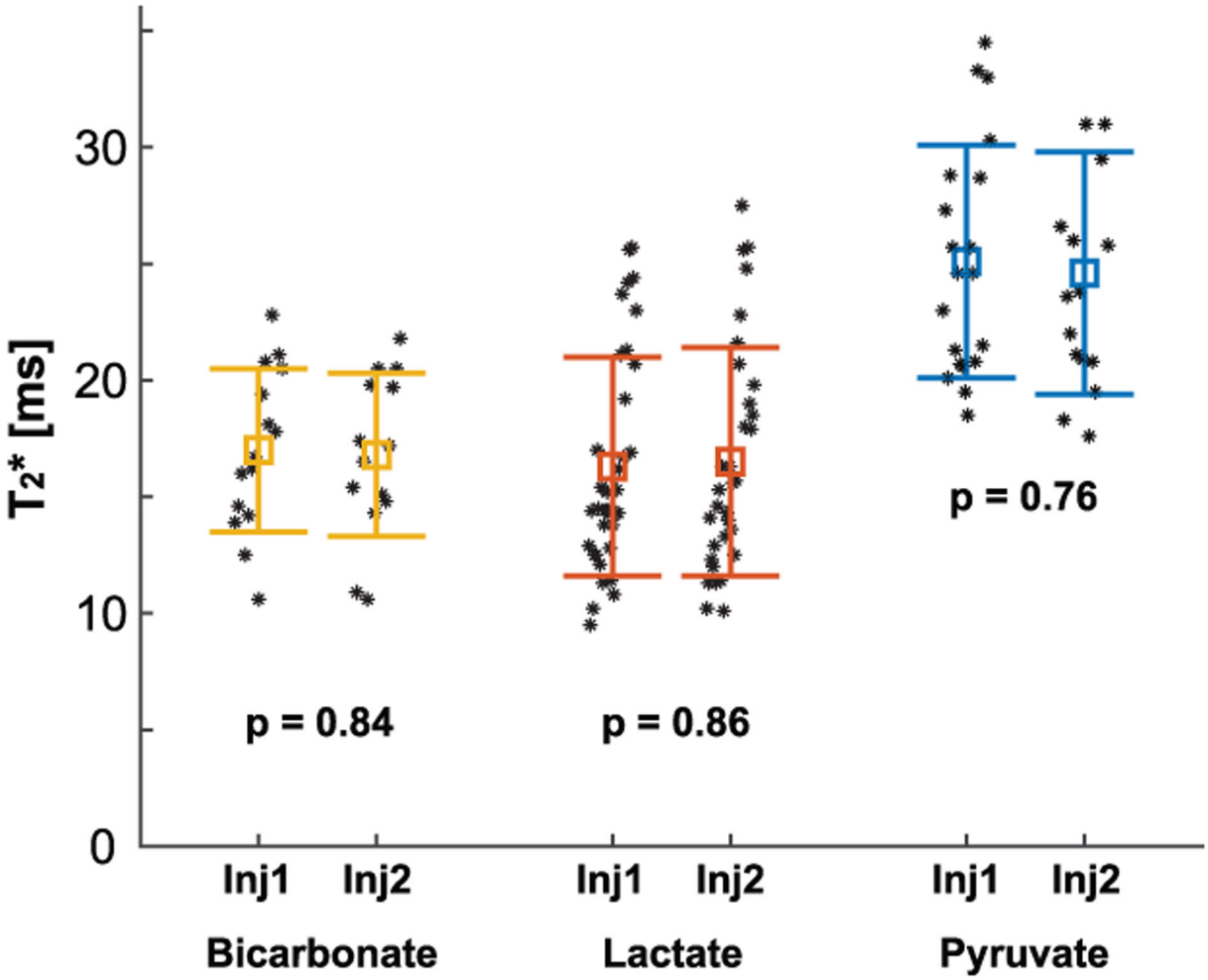

Figure 6. Reproducibility of T_2* measurements in rats.

T_2*s of the HP ^{13}C-metabolites measured from two consecutive HP [1-^{13}C]pyruvate injections were consistent ($p > 0.05$). Each marker represents a T_2* measurement from a single timepoint and the error bars denote the mean ± standard deviation.

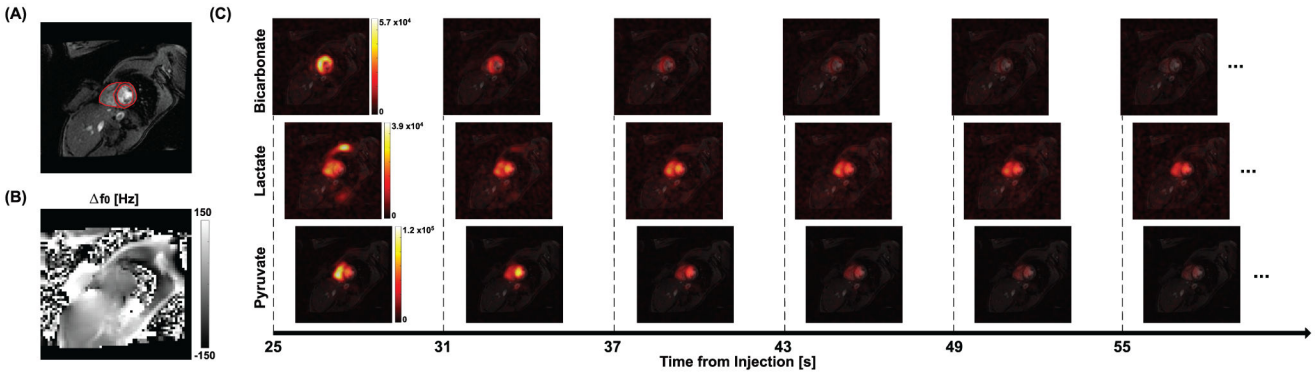

Figure 7. Hyperpolarized ^{13}C imaging from a healthy human subject.

(A) The prescribed SA plane for ^{13}C imaging (shown in ^{1}H MRI). (B) Δf_0 map of the corresponding slice. (C) Dynamic ^{13}C images (combination of 6 echoes) of HP [1-^{13}C]pyruvate, [1-^{13}C]lactate and [^{13}C]bicarbonate, acquired after an injection of HP [1-^{13}C]pyruvate.

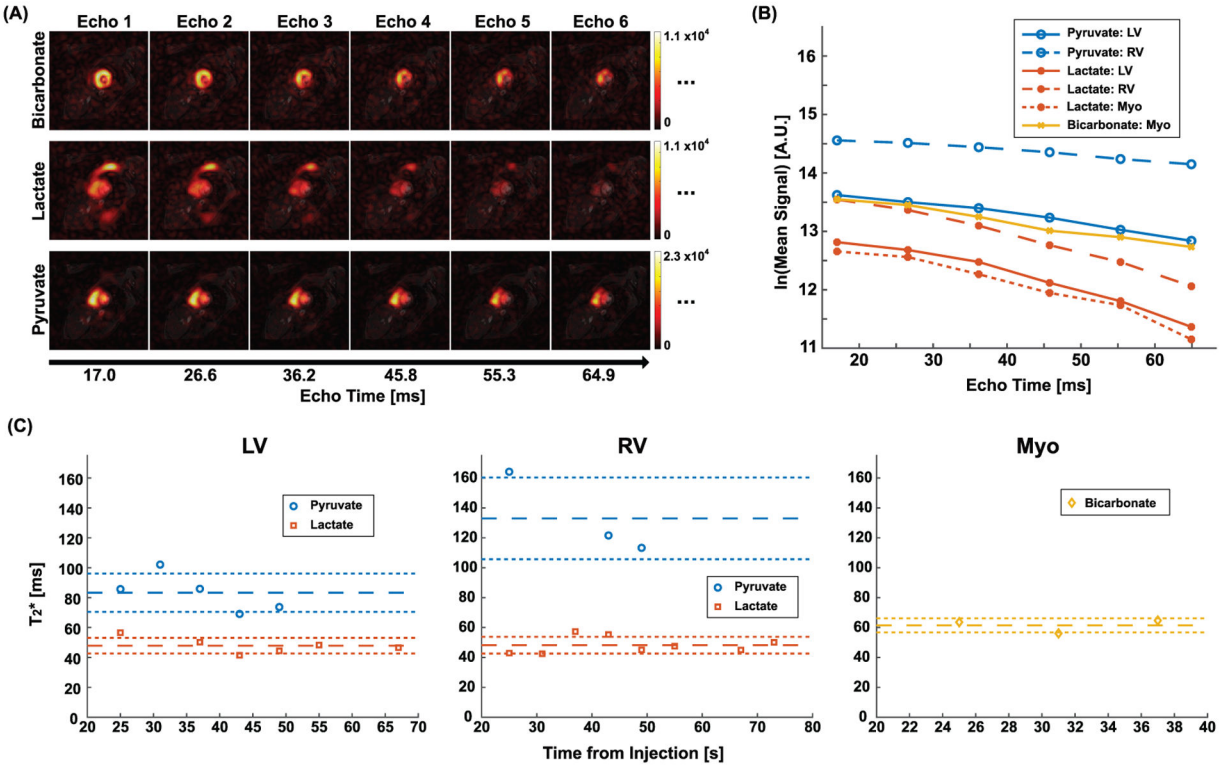

Figure 8. ***In vivo*** **cardiac T_2* measurement from the representative human subject.**

(A) Multiple echo images of HP [1-^{13}C]pyruvate, [1-^{13}C]lactate and [^{13}C]bicarbonate at 25 s post-injection. (B) Signal decays of HP signals in LV, RV, and Myo (ROIs are depicted as red contours in Fig. 7 (A)) along the echo time. (C) Dynamic changes of the T_2*s in the ROIs. The reference lines denote mean ± standard deviation.

Table 1.

Subject characteristics and compartmentalized time-averaged T_2*s of HP [1-^{13}C]pyruvate, [1-^{13}C]lactate and [^{13}C]bicarbonate.

Subject Demographics						Time-Averaged T_2* [ms]					
Subject ID	Sex	Age [years]	Height [cm]	Heart Rate [bpm]	Weight [kg]	[1-^{13}C]Pyr		[1-^{13}C]Lac			[^{13}C]Bic
						LV	RV	LV	RV	Myo	Myo
#1	F	38	172.7	72	55.0	83.3	133.0	47.9	48.2	46.2	61.5
#2	M	45	188.0	60	83.0	126.7	136.0	43.1	38.0	51.2	66.1
#3	F	48	152.4	64	61.1	116.1	119.3	31.7	46.5	33.7	65.5
Mean ± Standard Deviation						108.7 ± 22.6	129.4 ± 8.9	40.9 ± 8.3	44.2 ± 5.5	43.7 ± 9.0	64.4 ± 2.5